Theor Chem Acc (2017) 136:74
DOI 10.1007/s00214-017-2101-3

REGULAR ARTICLE

Microscopic analysis of AgCl polymorphism

Julia Contreras-García[1] · Miriam Marqués[2] · J. Manuel Recio[3]

Received: 27 January 2017 / Accepted: 7 May 2017 / Published online: 25 May 2017

Abstract A detailed theoretical study of the structural properties of the phases involved in the pressure-induced polymorphic sequence of AgCl is reported. As many other binary ionic compounds, AgCl crystallizes in the B1 (NaCl-type) structure at ambient pressure and shows a high-pressure B2 (CsCl-type) structure under pressure. However, unlike alkali halides, there is not a direct transformation from one to the other. The greater polarizability of the silver chloride structure enables the stabilization of two other phases in between B1 and B2: the monoclinic (KOH-type) and the orthorhombic (TlI-type, B33) structures. This polymorphic sequence is specially interesting, since a concerted transition pathway within the monoclinic KOH-type symmetry has also been proposed as a transition pathway in the B1 → B2 transformation. This would point at a connection between symmetries that are thermodynamically and kinetically stabilized, with phases that appear under pressure being good candidates for mechanistic analyses. Our calculations yield cell parameters and structural behavior under pressure in overall good agreement with available experimental data for all these phases and extend the information previously observed for the four polymorphs (e.g., compressibilities). Computed transition pressures confirm the B1→KOH-type→B33 sequence. In order to analyze the occurrence of the KOH-type phase between the B1 and B33 phases, we have resorted to the Atoms In Molecules approach to obtain the evolution of charges with pressure. We find that the descent to the KOH-type symmetry provides a continuous change in ionic charges between B1 and B33 phases, which implies a smaller stress. Thus, coupling group–subgroup relationships to chemical bond analysis can provide microscopic insight into why a given symmetry is favored.

Keywords Polymorphism · AgCl · Ionicity · AIM · Group–subgroup · High pressure

1 Introduction

Since pressure can introduce significant changes in the stability of phases, it is most useful in the synthesis of novel phases and metastable materials. Pressure allows precise tuning of a fundamental parameter, interatomic distance, which controls the electronic structure and virtually all the interatomic interactions that determine materials properties. With pressure tuning, properties can often be more rapidly and cleanly optimized than with chemical tuning, which necessitates the synthesis of a large number of different materials and can induce disorder, phase separation and other undesirable effects.

Pressure tuning is therefore a useful tool in the search for new solid-state materials with enhanced properties. This requires the comprehension of the inherent link between

Published as part of the special collection of articles derived from the 10th Congress on Electronic Structure: Principles and Applications (ESPA-2016).

✉ Julia Contreras-García
contrera@lct.jussieu.fr

[1] Laboratoire de Chimie Théorique (UPMC), Centre national de la recherche scientifique (CNRS), Tour 12-13, Bureau 420. CC137 - 4 place Jussieu, 75252 Paris Cedex 05, France

[2] SUPA, School of Physics and Astronomy, and Centre for Science at Extreme Conditions, The University of Edinburgh, Mayfield Road, Edinburgh EH9 3JZ, UK

[3] MALTA-Consolider Team and Departamento de Química Física y Analítica, Universidad de Oviedo, 33006 Oviedo, Spain

the macroscopic behavior of materials and the microscopic electronic organization. An in-depth understanding of the relationship between chemical structure and macroscopic behavior holds the key for rationalizing the design of new synthetic routes addressing a certain property. However, this requires the prediction of the stable phase at a given pressure–temperature condition. Evolutionary algorithms and metadynamics have provided an incredible advance in this direction [1–3]. However, the composition and a test number of atoms need to be provided in advance.

Moreover, the prediction of the stable phase of a solid does not provide insight into why a particular phase is the favored one. As pointed out by Hemley, "a fundamental yet empirically useful understanding of how pressure alters the chemistry of the elements is lacking" [4]. In this sense, analysis of polymorphic sequences can help to understand the factors that determine phase stability, as well as the enthalpic equilibrium between two phases at the transition pressure. Recently, the analysis of polymorphic sequences has been proposed as a way to get insight even into kinetic terms. It has been proposed that high-pressure phases are good candidates for intermediates in martensitic mechanisms [5, 6]. Thus, it becomes interesting to understand the polymorphic sequence of a solid and its link with its interactions at an atomic level.

Probably, the most common polymorphism in binary compounds is the B1→B2 transition undergone by most alkali halides, which has been thoroughly studied by one of our institutions [7–11]. Except for cesium halides, alkali halides crystallize in the B1 phase under ambient conditions, and the transition toward the B2 phase is known to happen for potassium and rubidium halides, as well as for NaF and NaCl. The transition of NaBr and NaI at 27 and 35 GPa, respectively, is less clear. Léger et al. [12] have proposed a TlI-type (B33) orthorhombic structure. Calculations by some of the authors have disentangled the origin of the preference of the B33 phase over the B2 due to the greater stability provided by the anionic polarizability in these compounds [13]. This proposal agrees with the appearance of the B33 phase in the polymorphic sequence observed in AgCl under pressure. Already in 1995, Kusaba et al. detected the transformation of the ambient B1 phase in AgCl toward a monoclinic $P2_1$ phase at ca. 6 GPa [14]. This phase transforms into the B33 at ca. 13 GPa. Further compression along with heating finally leads to the B2 phase (17 GPa, 473 K) [14]. Later X-ray data corrected the monoclinic group from $P2_1$ to $P2_1/m$ and provided numerous measures under pressure of phases B1, $P2_1/m$ (or KOH-type) and B33, which enable comparison with theoretical prediction [15]. Indeed, these transitions were confirmed from theoretical calculations by Catti et al. [16].

Whereas the above-cited alkali halides and their microscopic understanding are mainly governed by ionic interactions, the structure of more polar compounds such as AgCl is also dictated by other energetic terms and important covalent (exchange) contributions. This leads to a more complex polymorphic behavior, whose understanding can help building up the incomplete chemical intuition/laws under pressure. Silver halides constitute a big family of ionic, yet polar compounds. The appearance of the B33 phase in the polymorphic sequence of AgCl along with the possibility of using the $P2_1/m$ symmetry to describe the various phases (B1, B33 y B2) has recently been highlighted in the description of the transition mechanism from the B1 to the B2 phase [17–19]. The $P2_1/m$ symmetry has also been used to evaluate the mechanism in the B1→B2 transformation in NaCl [19] and AgCl [16]. With this in mind, it becomes interesting to analyze the thermodynamic aspects of the polymorphic sequence in AgCl and try to explain the evolution of the underlying chemical transformations, which has not yet been provided. Therefore, it is the main purpose of this paper to contribute to the microscopic understanding of the pressure-induced polymorphism of AgCl.

The rest of the paper is organized as follows. Firstly, we introduce the computational details. Then, the results and discussion section is divided into three subsections, which are devoted, respectively, to (i) the evaluation of the cohesive properties of each phase, (ii) the calculation of phase stability ranges and transition properties and (iii) the analysis of the evolution of bonding upon pressurization of each of the phases. The conclusions drawn from these results are summarized in the last section.

2 Computational details

All quantum-mechanical calculations have been made thanks to the VASP code (Vienna *ab initio* simulation package), [20] which solves the density functional theory (DFT) equations by means of plane waves and pseudopotentials with the implemented projected augmented wave formalism [21]. Within DFT, the electronic exchange and correlation are treated by using the generalized gradient approximation (GGA), in agreement with previous studies on the B1 phase of AgCl where the well-tested PW91 functional [22] proved to work better than other local density approximation functionals [23]. Convergence in computational parameters (cutoff energy (E_{cut}), k-points sampling, threshold energy in the self-consistent procedure) were thoroughly and independently checked in the B1 phase due to the high precision required in the analysis of relative stabilities. As a result, the Monkhorst-Pack k-points generation scheme was used with a $8 \times 8 \times 8$ grid (or analogous, according to the corresponding cell symmetries) in the first Brillouin zone. E_{cut} was set to 350 eV and the energy convergence to 10^{-3} eV. The optimization of the geometry at each volume was performed via a

conjugate gradient minimization of the total energy, using Hellmann-Feynman forces on the atoms and stresses on the unit cell. For the final energy calculation of the optimized crystal structure, the tetrahedron method with Blöch correction was applied.

The resulting total energy–volume per formula unit (E_i, V_i) calculated points of all AgCl polymorphs were described by means of numerical and analytical standard equations of state implemented in the GIBBS program [11]. Under the static approximation, zero temperature and zero-point vibrational contributions neglected, the Gibbs energy reduces to the enthalpy ($H = E + pV$) and this thermodynamic potential was evaluated to determine pressure ranges of stability of B1, KOH-type, B33 and B2 phases.

The topology of the electron density was calculated from the charge density obtained with VASP coupled to the CRITIC2 program [24] which enables both critical point location and basin integration. Relative errors in charge and volume integrations account to a maximum of 10^{-6} and 10^{-4} a.u., respectively.

3 Results and discussion

3.1 Cohesive properties

The conventional unit cells of the B1, KOH-type, B33 and B2 structures belong, respectively, to the $Fm\bar{3}m$, $P2_1/m$, $Cmcm$ and $Pm\bar{3}m$ space groups. The unit cell length a_c is the only parameter needed to describe the cubic B1 and B2 structures, whereas a_o, b_o, c_o, and the y_o coordinates of Ag and Cl determine the unit cell geometry of the orthorhombic B33 phase. For the KOH-type polymorph, cell parameters a, b, c, the cell angle β, and the x and z coordinates of Ag and Cl are needed to characterize its structure.

It is important to note that the polymorphs involved in the AgCl polymorphic sequence can be represented with a single common space group. Indeed, the monoclinic $P2_1/m$ space group of the KOH-type phase is a maximal common subgroup of all the other structures. Therefore, the conventional cells of B1, B33 and B2 structures can be understood as particular cases of the monoclinic $P2_1/m$ cell [16, 25].

This relationship will be especially interesting when comparing phases. Hence, transformations of the cell parameters and atomic positions from the reference (conventional) cells to the monoclinic one are collected in Table 1. Multiple equivalent coordinate transformations are available for the B1, B33 and B2 phases. Our selection has only been made on the basis of the similarity between adjoining phases and of the reduction of computational time in our geometrical optimization strategies.

We have performed extensive total energy calculations for the four AgCl polymorphs at selected volumes around $V_0(\text{exp}) = 42.65$ Å^3, the observed value of the B1 phase at ambient conditions [15]. Our strategy started with a full geometrical optimization of the monoclinic unit cell in the volume range 26–50 Å^3. Due to the large number of parameters involved in the energy minimization of the KOH-type unit cell $(a, b, c, \beta, x_{\text{Ag}}, z_{\text{Ag}}, x_{\text{Cl}}, z_{\text{Cl}})$, several numerical problems have been observed. As an example, we found difficulties to locate the absolute energy minimum at volumes in the neighborhood where the higher-symmetry structures display similar energies. Then, we decided to recalculate (E_i,V_i) points for the B1, B33 and B2 structures using: (i) the monoclinic cell but taking into account the geometrical constrains imposed by the cubic and orthorhombic lattices and (ii) their corresponding conventional cells.

Table 1 Cell parameters in the monoclinic reference frame in terms of the cubic (c) and orthorhombic (o) ones for the B1, B2 and B33 structures

	$Fm\bar{3}m$	$Cmcm$	$Pm\bar{3}m$
	a_c	a_o, b_o, c_o	a_c
a	$a_c/\sqrt{2}$	a_o	a_c
b	$a_c/\sqrt{2}$	c_o	$a_c\sqrt{2}$
c	a_c	$b_o/(2\sin\beta)$	$a_c\sqrt{2}$
β	90°	$90° + \tan^{-1}(a_o/b_o)$	90°
x_{Ag}	0.25	$y_{\text{Ag},o}$	0.00
z_{Ag}	0.25	$2y_{\text{Ag},o}$	0.25
x_{Cl}	0.25	$y_{\text{Cl},o}$	0.50
z_{Cl}	0.75	$2y_{\text{Cl},o}$	0.75

Please note that several equivalences do exist for some of the cells

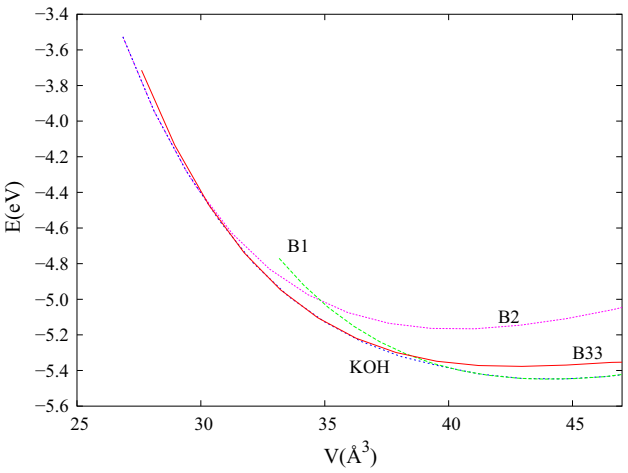

Fig. 1 Energy–volume curves for the B1, KOH-type, B33 and B2 polymorphs of AgCl according to our GGA calculations. It can be seen how the energy of the KOH-type structure coincides with that of the *cubic* and *orthorhombic* lattices at different volume ranges

Table 2 Zero-pressure cohesive properties of B1, KOH-type, B33 and B2 polymorphs according to our static GGA calculations. All structural data are referred to the monoclinic cell

	B1	KOH-type	B33	B2
a(Å)	3.97	3.97	3.80	3.43
b(Å)	3.97	3.97	3.91	4.85
c(Å)	5.61	5.62	6.05	4.85
β(°)	90.0	90.1	108.2	90.0
V_0(Å^3)	44.1	44.3	42.7	40.3
x_{Ag}	0.250	0.249	0.394	0.000
z_{Ag}	0.250	0.250	0.788	0.250
x_{Cl}	0.250	0.251	0.133	0.500
z_{Cl}	0.750	0.750	0.267	0.750
ΔE_0(kJ/mol)	0	0.14	6.83	27.07

Curves connecting the computed (E_i,V_i) points for each polymorph are depicted in Fig. 1. The curve for the KOH-type polymorph overlaps with the curves of the other phases at particular volume ranges. Furthermore, going from high to low volumes, this energy coincidence follows the sequence B1, B33 and B2, i.e., the same polymorphic sequence found in high-pressure experiments [14, 15].

Zero-pressure structural parameters and energies relative to the B1 phase (ΔE_0) of the four polymorphs are collected in Table 2. Structural data are expressed in terms of the $P2_1/m$ symmetry following Table 1. Positive ΔE_0 values for B33 and B2 indicate that our simulations found the B1 phase as the thermodynamically stable phase at ambient conditions, which agrees with the experimental behavior. As discussed above, the KOH-type structure collapses into the B1 phase at this geometry, the slight differences between the structural properties and energies of B1 and KOH type at zero pressure being due to the difficulty highlighted above of converging to higher-symmetry structures. Notice also that the polymorphic sequence agrees with what is expected from

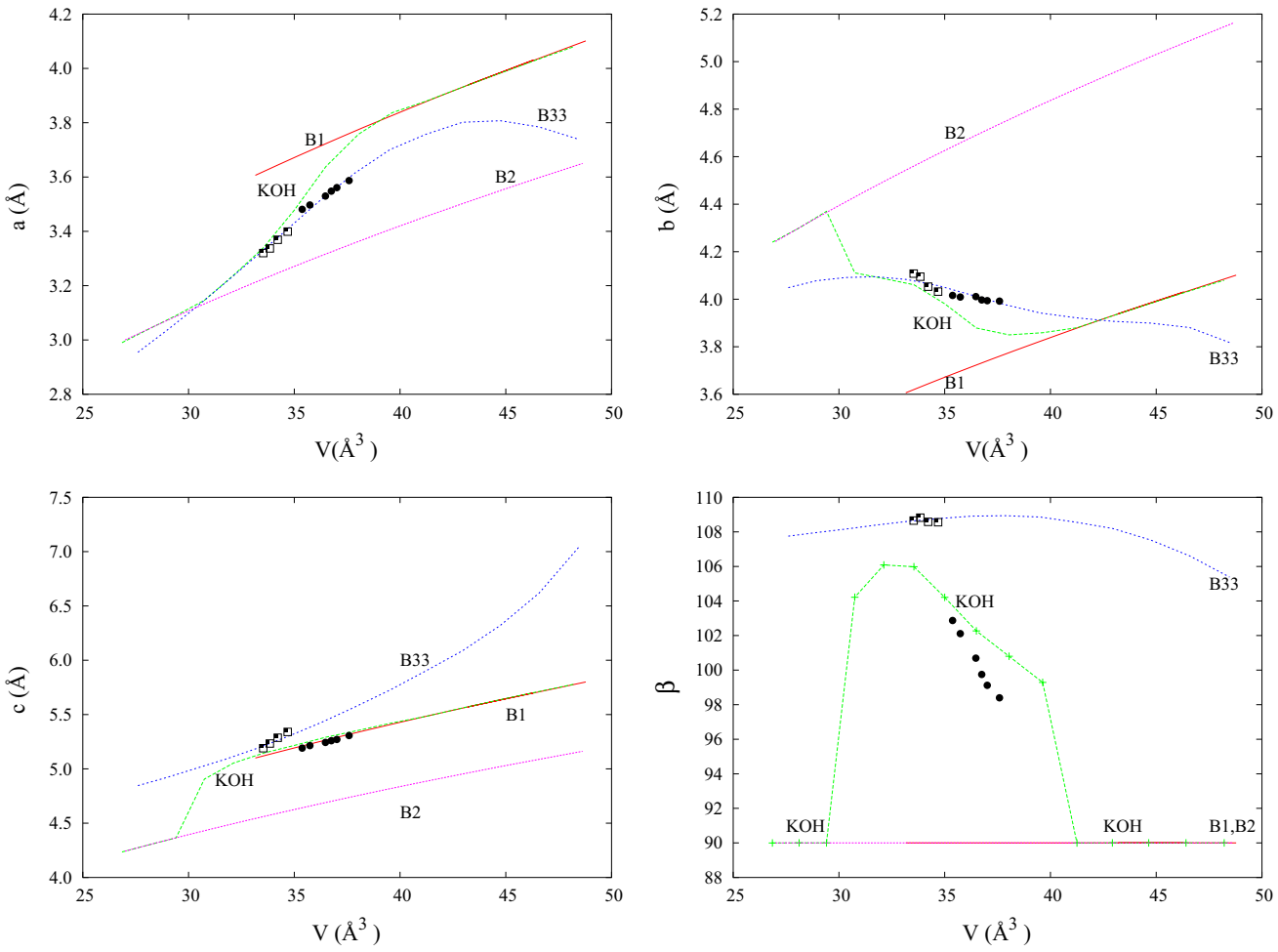

Fig. 2 Variation of the unit cell parameters with volume according to our GGA calculations (*solid lines*) and available experimental data (*symbols*) [15]. *Black dots* and *white squares* stand, respectively, for the KOH-type and *B*33 structures. All data referred to the $P2_1/m$ unit cell

the relative E and V values of the phases. For example, ΔE_0 is greater for B2 than for B33 (Table 2).

Only the geometry of the B1 phase is experimentally accessible at zero pressure. Our calculated static result $a_c = 5.61$ Å is very close to the observed lattice parameter $a_c = 5.546$ Å at room temperature [15]. At increasing pressures, the agreement between our calculated values and the experimental ones of Kusaba et al. [14] (in brackets) is also very satisfactory (Fig. 2). For example, the cell parameters of the KOH-type structure at 9 GPa are $a = 3.661$ (3.516), $b = 3.895$ (3.988), $c = 5.320$ (5.225), $\beta = 102°$ (101°), and those of the B33 structure at 13.5 GPa are $a = 3.424$ (3.350), $b = 10.057$ (9.916), $c = 4.057$ (4.093) (lengths in Å and angles in degrees). We can extend the comparison to the atomic coordinates of the two non-cubic structures (the other ones having fixed Wyckoff positions). Representative results are depicted in Fig. 3. They include the volume dependence of x_{Ag} and z_{Ag} coordinates in KOH-type and B33 structures. The calculated lines for the monoclinic structure illustrate the continuous evolution of these coordinates from the B1 limit at high volumes ($x_{Ag} = z_{Ag} = 0.25$) to the B2 limit at low volumes ($x_{Ag} = 0$ and $z_{Ag} = 0.25$). In the intermediate range of volumes, the optimized Ag positions are consistent with the observed values of the KOH-type phase [15]. A good agreement between theory and experiment is found if we look at the calculated atomic coordinates in the B33 phase. They show an almost negligible variation in the whole volume range with the experimental values lying very close to the computed curves. An analogous picture has been obtained for the internal coordinates of Cl.

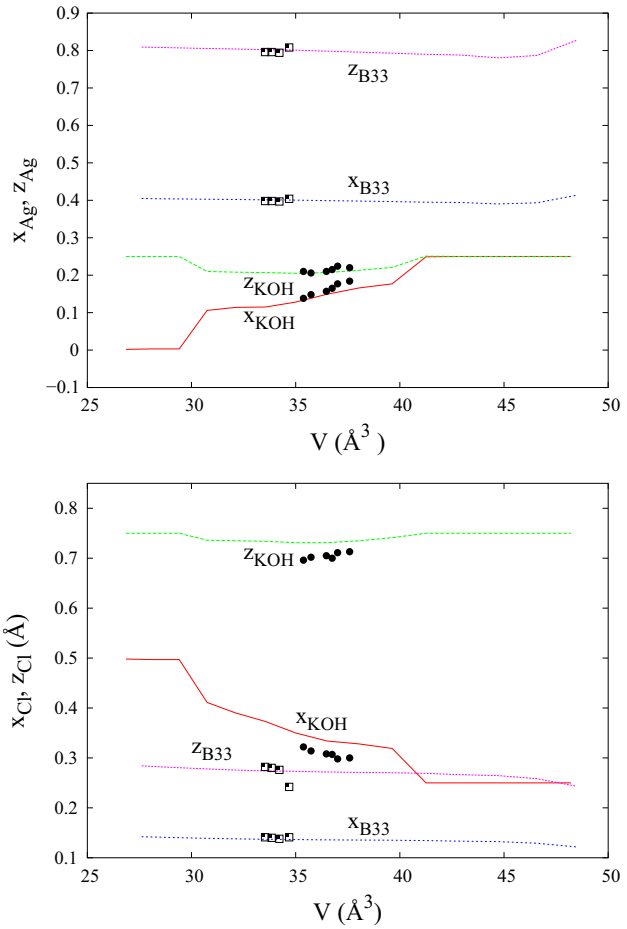

Fig. 3 Variation of Ag position with volume according to our GGA calculations (*solid lines*) and available experimental data (*symbols*) [15]. *Black dots* and *white squares* stand, respectively, for the KOH-type and B33 structures. All data referred to the $P2_1/m$ unit cell

3.2 Transition properties

As regards the stability pressure ranges of the four observed polymorphs of AgCl, we have calculated the equilibrium transition pressures (p_t) in the static approximation by solving for the pressure that provides the same Gibbs energy (H at zero temperature) for both phases. Numerical data associated with the phase transitions are provided in Table 3. It can be seen that our results are in overall agreement with previous studies, both in the transition pressures and in the order of magnitude of the cell volume changes at p_t.

It is interesting to point out that some of the observed transitions involve phases with a group–subgroup relationship. This is the case of the B1 → KOH-type and the KOH-type → B33 transformations. Computationally, this fact is reflected by a continuous and soft approach or divergence of the corresponding Gibbs energy–pressure curves (see

Table 3 Comparison of our theoretical transition pressures and relative volume changes at p_t with those calculated by Nunes et al. [26] (Cal-N) and Catti [16] (Cal-C) and those experimentally obtained at ambient temperature by Kusaba et al. [14] (Exp-K), and Hull and Keen [15] (Exp-H)

	This work	Cal-N	Exp-K	Exp-H	Cal-C
B1 → KOH	3.3	–	~ 8	6.6	3.5
	−1.04	–	−3.3⋆	−1.6	
KOH→ B33	12.0	–	~ 13	10.8	6.0
	−0.72	–	−1.0⋆	−1.9	
B33 → B2	32.5	–	17†–13.5‡	–	17.7
	−2.22	–	−0.7⋆	–	
KOH → B2	33.6	–	–	–	
	−0.95	–	–	–	
B1 → B2	14.8	11	–	–	
	−7.29	−7.14	–	–	

For each transition, pressures (GPa) in the first row and percentual relative volumes in the second row

$^{\dagger}T = 473$ K

$^{\ddagger}T = 573$ K

⋆ Estimated values

Fig. 4) that replace the usual crossing point associated with first-order transitions. This picture could lead to a misunderstanding of the nature of the transitions and to consider that some of them are of second-order type. However, small volume changes are obtained for this kind of transformations at their corresponding transition pressures.

The p_t value predicted for the B33 → B2 is too high, whereas previous static simulations by Catti [16] obtained very similar results to those of Kusaba et al. [14]. However, we consider that our prediction should not be taken as anomalous, since the experimental data were obtained at finite temperatures (200 °C) and they point toward a negative Clapeyron slope ($\frac{dp_t}{dT}$). In fact, a linear extrapolation of the experimental data gives an approximate value of 33.6 GPa for the transition pressure at the athermal limit, considerably close to our result.

It should be noted that it has been especially difficult to determine which phase preludes the B2 phase due to the competition between the B33 and the KOH-type phases. According to our calculations, the B33 → B2 transition would not take place directly. Instead, a slight decrease in symmetry is observed prior to the B2 phase. This possibility was not analyzed in previous simulations [16], and since it falls within the chemical accuracy of functionals, we decided to further dwell on it through the analysis of the chemical changes involved.

3.3 Changes in bonding

We have analyzed the chemical changes involved in the pressurization of the phases in order to analyze the role of the KOH-type phase along the B1 → KOH-type → B33 transition sequence.

In order to quantitatively investigate the evolution in bonding and charge separation, we have carried out the topological analysis of the electron density. This approach, also known as the Quantum Theory of Atoms In Molecules (QTAIM) [27], enables to divide the solid system into its component atoms with well-defined volumes. Thus, properties such as charge or volume can be obtained by integration within these volumes [28–31].

Figure 5a shows the resulting charges (q) as pressure is applied for Ag and Cl. It can be seen that this approach provides indeed a greater charge separation (ionicity) for the B2 than the B1 phase, in agreement with the expected result. However, this is not the case for the less symmetric phases. In B33, a smaller charge transfer is observed all throughout, and the low symmetry of the KOH-type cell enables a great variation upon pressurization. Results for the KOH-type phase from direct calculation (not leading to high-symmetry phases) are shown in order to follow the minimum stress path.

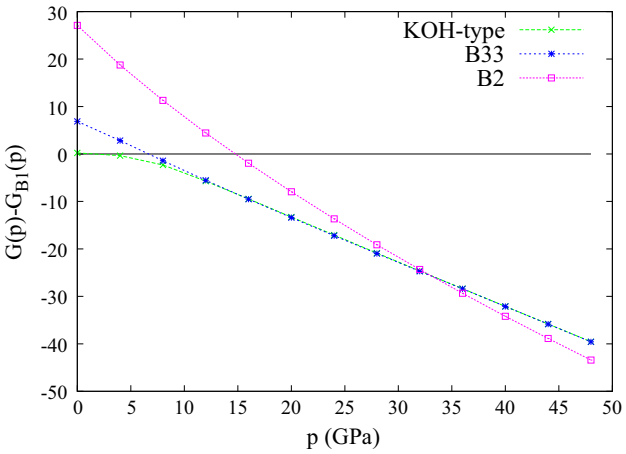

Fig. 4 Gibbs energy of KOH-type, B33, and B2 polymorphs relative to B1 vs. pressure

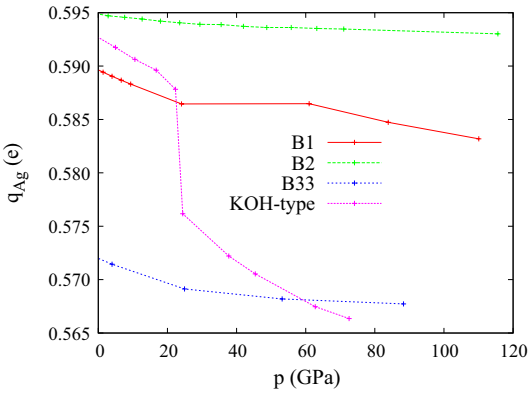

Fig. 5 Evolution of Bader charges upon compression in the B1, B2, B33 and KOH-type phases

Figure 5a yields two important conclusions that affect polar ionic compounds such as AgCl and why they can present richer polymorphic sequences. On the one hand, the $P2_1/m$ symmetry not only links the B1 and the B33 phases from the symmetric point of view. It also does so from the chemical point of view. Indeed, KOH-type charges evolve from the ones in the B1 phase at low pressures to those of the B33 phase as pressure increases. Hence, the descent in symmetry toward the KOH-type phase allows chemical changes to proceed smoothly from the B1 to the B33 phase, instead of doing so abruptly, which would lead to a greater stress. On the other hand, this approach enables to explain the absence of the B33 phase in the polymorphic sequence of more ionic compounds such as most alkali halides. The distortion toward the *Cmcm* phase leads to a smaller charge separation, which is only possible in less ionic compounds and/or polarizable ions.

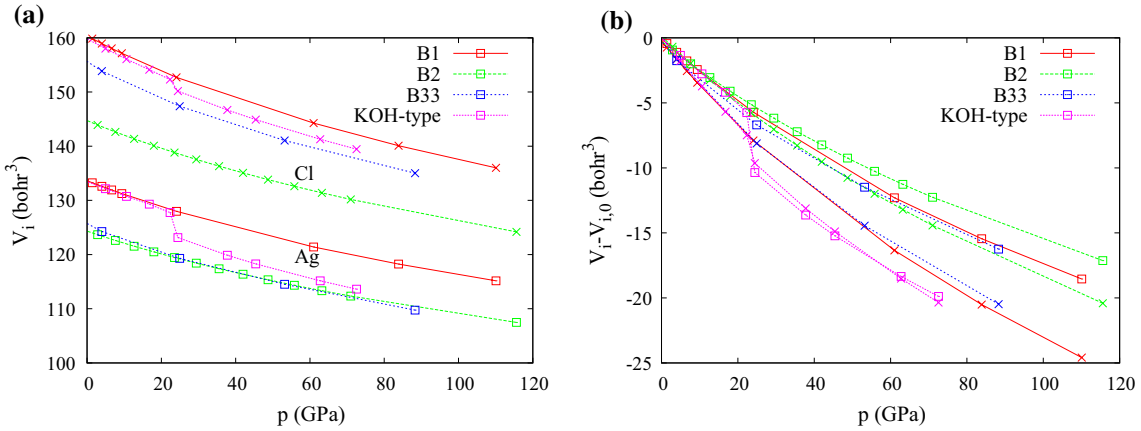

Fig. 6 **a** Evolution of Bader volumes V_i upon compression in the B1, B2 B33 and KOH-type phases. **b** $\Delta V_i = V_{i,p} - V_{i,0}$ for each of the previous phases. Ag in *squares* and Cl in *crosses*

All in all, the descent to the KOH-type symmetry provides a continuous change in atomic charges between B1 and B33 phases, which implies a smaller stress. Thus, coupling group–subgroup relationships to chemical bond analysis can provide microscopic insight into why a given symmetry is favored. Finally, making use of the results from the integration, we can also analyze how the compression of each phase takes place. Figure 6a shows the evolution of Bader volumes upon pressurization. It can be seen that the phase volumes correspond to the compression principle expected under pressure that we had already seen in the analysis of zero-pressure volumes: B1 volume is greater than B33, and B33 is greater than B2 (see Table 2) [32]. Again, the KOH-type phase is found to link the behavior of the B1 and B33 phases.

Moreover, the separation into atoms enables to show that in phases B1, B2 and B33 the chlorine atom, softer than Ag, is the one mainly being compressed. This is made clearer in Fig. 6b, where we have plotted $\Delta V_i = V_{i,p} - V_{i,0}$ for each of the previous phases.

4 Conclusions

The structural properties of all the observed polymorphs of AgCl have been determined in good agreement with the available experimental data. We must highlight the optimal agreement of the atomic coordinates, which enable us to consider our computational choices can recover the relative stability of phases along with their transition pressures.

Our calculations have reproduced the observed polymorphic sequence of AgCl with reasonable transition pressures and volume collapses, though a competition between the KOH-type and the B33 phases has been observed when transitioning to the B2 phase. The changes in volume at the transition pressures are close to the experimental ones and in all cases low enough as to expect small energy barriers and hysteresis cycles.

From the Atoms In Molecules point of view, the KOH-type phase is found to lead to a chemical connection in terms of charges between the B1 and B33 phases. Thus, its appearance can be understood as a way to reduce the stress that a direct transformation would imply. With these conclusions, we want to underline the relevance of coupling group theory and chemistry in the analysis of phase transitions.

Acknowledgements Financial support from Principado de Asturias (GRUPIN14-049) and the Spanish MINECO Projects (CTQ2015-67755-C2-R and MAT2015-71070-REDC) is gratefully acknowledged.

References

1. Glass CW, Oganov AR, Hansen N (2006) Comput Phys Comm 175:713
2. Lonie DC, Zurek E (2011) Comput Phys Commun 182:372
3. Martonak R, Laio A, Bernasconi M, Ceriani C, Raiteri P, Parrinello M (2005) Z Krist 220:489
4. Hemley RJ (2010) High Press Res 30:581
5. Contreras-Garcia J, Silvi B, Recio JM (2011) Modern charge density analysis. Springer, ISBN 978-90-481-3835-7
6. Boto RA, Marques M, Beltran A, Andres J, Riffet V, Labet V, Contrersas-Garcia J, (2016) An introduction to high-pressure science and technology. CRC Press, ISBN 9781498736220
7. Recio JM, Martín Pendás A, Francisco E, Luaña V (1993) Phys Rev B 48:5891
8. Martín Pendás A, Luaña V, Recio JM, Flórez M, Francisco E, Blanco MA, Kantorovich LN (1994) Phys Rev B 49:3066
9. Martín Pendás A, Recio JM, Francisco E, Luaña V (1997) Phys Rev B 56:3010
10. Flórez M, Recio JM, Francisco E, Blanco MA, Martín Pendás A (2002) Phys Rev B 66:144112

11. Blanco MA, Francisco E, Luaña (2004) Comp Phys Comm 158:57
12. Léger CJM, Haines J, Oliveira LS (1998) J Phys Condens Matter 10:4201
13. Marques M (2001) Efectos de polarización en la predicción de estructuras ortorrómbicas en haluros alcalinos. Universidad de Oviedo, Seminario de Investigación
14. Kusaba K, Syono Y, Kikegawa T, Shimomura O (1995) J Phys Chem Solids 56:751
15. Hull S, Keen DA (1999) Phys Rev B 59:750
16. Catti M, Di Piazza L (2006) J Phys Chem B 110:1576
17. Tolédano K, Knorr K, Ehm L, Depmeier W (2003) Phys Rev B 67:144106
18. Stokes HT, Hatch DM, Dong J, Lewis JP (2004) Phys Rev B 69:174111
19. Catti M (2004) J Phys Condens Matter 16:3909
20. Kresse G, Furthmuller J (1996) Phys Rev B 54:11169
21. Kresse G, Joubert J (1999) Phys Rev B 59:1758
22. Perdew JP, Wang Y (1992) Phys Rev B 45:13244
23. Oyoke CMI (2002) Phys Status Solidi B 234:580
24. Otero-de-la-Roza A, Johnson ER, Contreras-García J (2012) Phys Chem Chem Phys 14:12165
25. Stokes HT, Hatch DM (2002) Phys Rev B 65:144114
26. Nunes GS, Allen PB, Martins JL (1998) Phys Rev B 57:5098
27. Barder RFW (1990) Atoms in molecules. A quantum theory. Clarendon Press, Oxford
28. Gatti C (2005) Z Krist 220:399
29. Pereira ALJ, Gomis O, Sans JA, Contreras-García J, Manjon FJ, Rodriguez-Hernandez P, Munoz A, Beltran A (2016) Phys Rev B 93:224111
30. Contreras-García J, Martín Pendás A, Recio JM (2008) J Phys Chem B 112:9787
31. Contreras-García J, Martín Pendás A, Silvi B, Recio JM (2009) J Phys Chem B 113:1068
32. Contreras-García J, Mori-Sanchez P, Silvi B, Recio JM (2009) J Chem Theor Comp 5:2108